Ivan Korade, Zdravko Virag and Mario Šavar

Numerical Simulation of One-dimensional Blood Flow in Elastic and Viscoelastic Arterial Network

University of Zagreb, Faculty of Mechanical Engineering and Naval Architecture

Introduction

Numerical simulation of blood flow in the arterial tree is challenging due to difficulties in describing the gemetry, nonlinear wall viscoelasticity, and non-Newtonian rheological properties of blood. One-dimensional models present a good compromise between Windkessel and three-dimensional models [1, 2]. Numerical simulation of arterial flow is very useful for the thorough understanding of pressure and flow waves propagation phenomena.

The goal of this paper is to present a method of characteristics (MOC) [3, 4] for solving a nonlinear one-dimensional model in an arterial tree with elastic and viscoelastic wall. The developed method was applied to the 37-element silicone model of arterial tree with available experimental data [5]. The test was used in [6] to check the ability of the mathematical model and the numerical scheme of correctly describing the multiple reflections from multiple outflow and junction conditions. Here we used this benchmark to verify the in-house developed code by comparing the obtained results with the experimental data and with the results of other methods.

Mathematical model

A one-dimensional model of blood flow in a pipe with viscoelastic wall reads [6]:

$$\frac{\partial A}{\partial t}+\frac{\partial Q}{\partial x}=0\,, \tag{1}$$

$$\frac{\partial Q}{\partial t}+\frac{A}{\rho}\frac{\partial p}{\partial x}+\frac{\partial (Qv)}{\partial x}=-fQ\,, \tag{2}$$

$$p - p_0 = \frac{1}{C_D}(\sqrt{A} - \sqrt{A_0}) + \eta\frac{\partial A}{\partial t}, \tag{3}$$

where x, t are the space and the time coordinate, respectively, A is cross-sectional area ($A = D^2\pi/4$), Q is volume flow rate, and $v = Q/A$, p is transmural pressure, ρ is fluid density, A_0 is constant cross-sectional area at a constant pressure of p_0. Coefficients f, C_D and η are defined by:

$$f = \frac{2(\zeta+2)\pi\mu}{\rho A},\ C_D = \frac{3A_0}{4\sqrt{\pi}E\delta} \text{ and } \eta = \frac{\tau}{2C_D\sqrt{A}}, \tag{4}$$

where μ is fluid viscosity, ζ is constant for particular velocity profile, E is elastic modulus and τ is retardation time constant in the Voigt model.

Numerical method

The artery is discretized into a number of elements of length Δx. Fig. 1 shows two typical elements (denoted by j and k) bounded by nodes (I, J, and K). The pressure is defined at the nodes, A is defined in the middle of each element (and it is considered to be constant along the element) and Q is defined at each end of each element. Thus, four unknowns are stored for each element. For example, the unknowns related to the element j are p_J, Q_{jL}, Q_{jD} and A_j, as shown in Fig. 1.

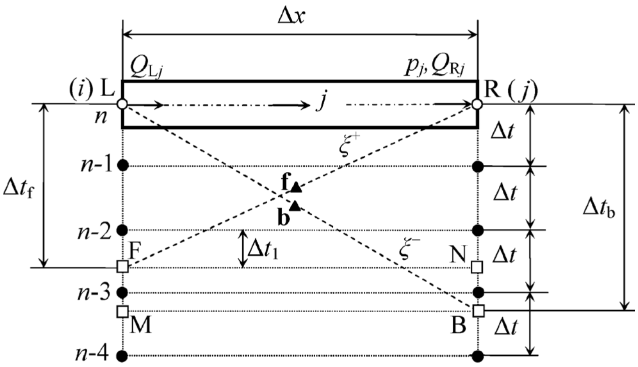

Fig. 1. An element of a discretized arterial tree with the arrangement of variables. For each element, three variables are stored: pressure p_j, flow rate Q_{Rj} at the element outlet, and Q_{Lj} at the element inlet. The time instances are denoted by n, n-1, n-2, n-3, and n-4. Dashed lines denote the characteristics defined by $\xi^+ = v + c$ and $\xi^- = v - c$; empty circles denote the nodes at the new instance at which unknowns should be calculated; filled circles denote nodes at older time instances at which the values of all variables are known from the previous integration steps; squares denote the interpolation points F and B on the forward and backward characteristic lines, and the auxiliary interpolation points N and M are at the same time instances as the points F and B, respectively; triangles denote midpoints f and b of the forward and backward characteristics, respectively

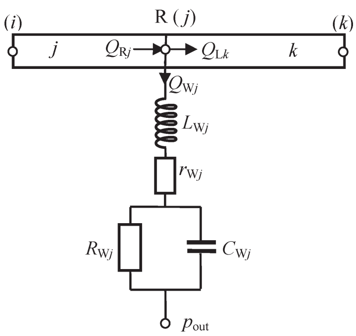

Fig. 2. Electrical analogue scheme of the Windkessel model defining the node outlet boundary condition

By using Eq. (3), Eqs. (1) and (2) can be transformed into a set of compatibility equations, which are valid along two characteristic lines defined by $\xi^{\pm} = v \pm c$ in the form:

$$\frac{1}{C}\mathrm{d}Q^{\pm} - (v \mp c)\mathrm{d}p^{\pm} = = -\frac{1}{C}fQ\mathrm{d}t - v^2\eta\frac{\partial^2 A}{\partial x \partial t}\mathrm{d}t + (v \mp c)\eta\frac{\partial^2 Q}{\partial x \partial t}\mathrm{d}t, \tag{5}$$

where $C = 2C_D\sqrt{A}$, and $c = \sqrt{A/(\rho C)}$ is wave speed. We establish relationship between pressure and area from the discretized form of Eq. (3), which serves to exclude A from the set of unknowns. The third equation related to each node is the continuity equation. For example, at node R in Fig. 2, this equation reads:

$$Q_{Rj} = Q_{Wj} + \sum_{k=1}^{N_{out}} Q_{Lk}, \tag{6}$$

where Q_{TJ} is the branching flow from the large artery into a small one, which is modeled by the inertial four element Windkessel as depicted in Fig. 2. In this model, L_J is inertance, r_J is resistance, C_{TJ} is the capacity of branching arteries and R_J is the peripheral resistance at node J.

We discretized Eq. (5) and all other auxiliary equations by using second order accuracy, and the resulting system of algebraic equation is solved by a direct method. The

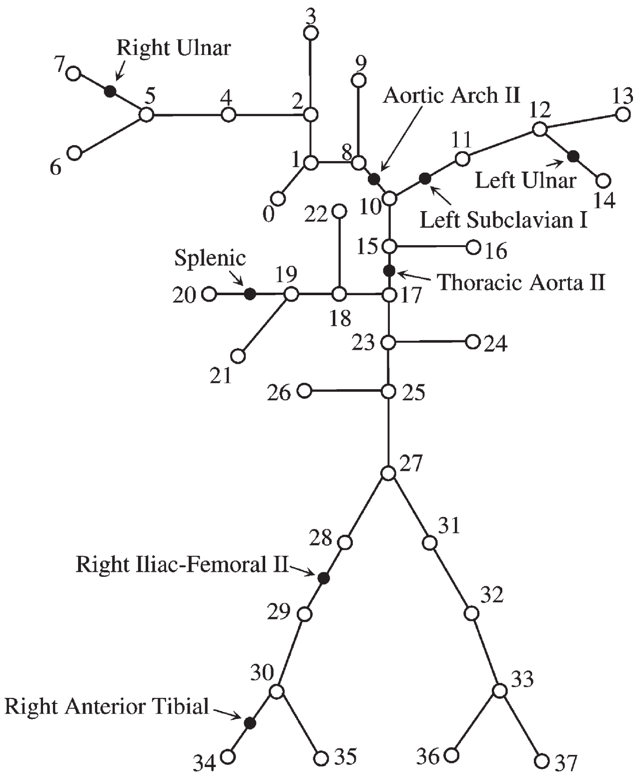

Fig. 3. Scheme of 37-segment arterial tree. The node number zero denotes the arterial tree inlet, where a periodic flow rate was prescribed. Filled circles denote measurement sites

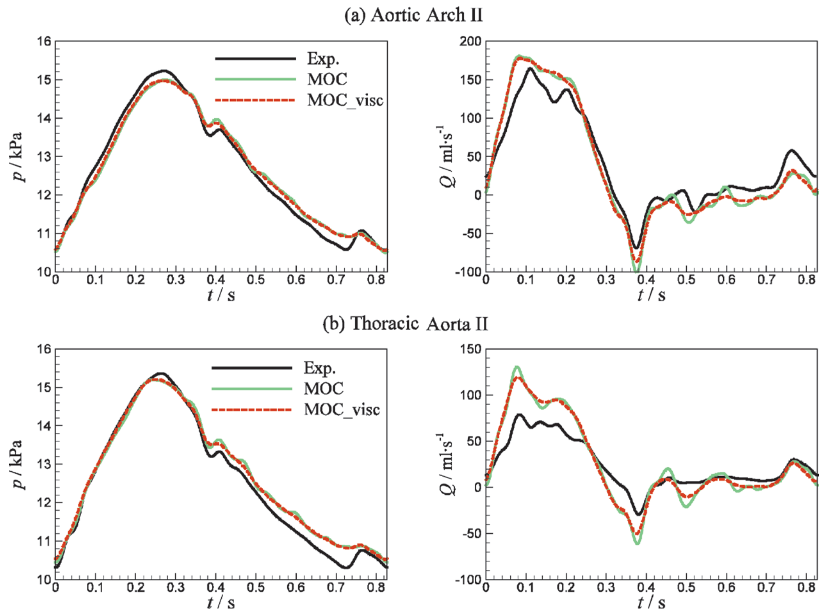

Fig. 4. 37-artery network. Pressure (left) and flow rate (right) at midpoints of two arterial segments: (a) Aortic Arch II and (b) Thoracic Aorta II. Black solid lines represent in vitro experimental data (Exp.), green solid lines denote numerical results of the developed method with elastic arterial wall (MOC), and red dashed lines denote numerical results of the method of characteristics with viscoelastic arterial wall (MOC_visc) [4]

Table 1. Percentage RMS errors of the calculated pressure and flow rate with respect to the measurements at the locations indicated in Fig. 3, and the range of these errors from six other numerical schemes

Arterial segment	Numerical scheme		ε_p^{RMS}	ε_Q^{RMS}
Aortic arch II	Six schemes	min	1.68	12.02
		max	1.94	12.34
	MOC		1.77	12.47
	MOC – visc.		1.56	11.89
Thoracic aorta II	Six schemes	min	2.17	25.26
		max	2.53	25.62
	MOC		2.26	26.27
	MOC – visc.		2.15	24.50
Left subcl. I	Six schemes	min	3.05	13.87
		max	3.12	14.45
	MOC		3.19	14.39
	MOC – visc.		3.04	13.53
R. iliac-femoral II	Six schemes	min	3.65	23.90
		max	3.97	24.80
	MOC		3.97	26.02
	MOC – visc.		3.68	22.52
Left ulnar	Six schemes	min	2.57	12.42
		max	2.75	12.91
	MOC		2.67	12.81
	MOC – visc.		2.28	11.36
R. anter. tibial	Six schemes	min	3.21	9.88
		max	3.43	11.05
	MOC		3.90	10.98
	MOC – visc.		3.15	8.15
Right ulnar	Six schemes	min	2.42	11.22
		max	2.66	11.73
	MOC		2.62	11.84
	MOC – visc.		2.53	10.70
Splenic	Six schemes	min	2.22	9.02
		max	2.36	9.79
	MOC		2.52	10.37
	MOC – visc.		1.93	7.80

method is implicit, unconditionally stable and capable of dealing with nonlinearities.

At the inlet node the pressure or the inflow can be prescribed. In all simulations, the initial conditions were $Q(x,0)=0$, $A(x,0)=A_0$ and $p(x,0)=p_0$. The integration time should be long enough to achieve cycle-to-cycle periodicity, and the last cycle is examined.

Results and discussion

Fig. 3 schematically shows the examined network. All data relevant to this problem are provided in the supplement material [6]. In the performed simulation each segment was divided into a number of elements (total number of elements was 431), and integration time step was 1 ms. Fig. 4 shows the comparison of the measured and calculated pressure and flow (for the case of elastic and viscoelastic wall), and Table 1 shows the percentage root mean square (RMS) errors of the calculated results with respect to the experimental data of the developed method and the range of these errors from the six other methods examined in [6].

In the case of elastic wall, most of the MOC errors are very similar in size to errors from six numerical schemes (see Table 1). In the case of viscoelastic wall, the pressure and flow RMS errors are slightly reduced, and a reduction in peak values of pressure and flow rate is achieved (that is closer to experimental data) because of damping high frequency oscillations.

References

[1] Ottesen, JT, Olufsen, MS, Larsen, JK. *Applied mathematical models in human physiology*. SIAM: Society for Industrial and Applied Mathematics, 2004.

[2] van de Vosse FN, Stergiopulos N. Pulse wave propagation in the arterial tree. *Annual Review of Fluid Mechanics* 2011; **43**(1): 467–499. DOI: 10.1146/annurev-fluid-122109-160730.

[3] Korade I, Virag Z, Šavar M. Numerical simulation of one-dimensional flow in elastic and viscoelastic branching tube. *Proceedings of the 6th European Conference of Computational Fluid Dynamics (ECFD VI)*, Oñate E, Oliver X, Huerta A (ur). International Center for Numerical Methods in Engineering (CIMNE): Barcelona, Spain, July 20-25, 2014; 7124–7131.

[4] Korade I, Modeliranje strujanja krvi u arterijskom stablu s viskoelastičnom stijenkom (eng. Modeling of Blood Flow in an Arterial Tree with Viscoelastic Wall), PhD, University of Zagreb, Faculty of Mechanical Engineering and Naval Architecture, 2017.

[5] Matthys KS, Alastruey J, Peiró J, Khir AW, Segers P, Verdonck PR, Parker KH, Sherwin SJ. Pulse wave propagation in a model human arterial network: Assessment of 1-D numerical simulations against in vitro measurements. *Journal of Biomechanics* 2007; 40 (15):3476–3486. doi:10.1016/j.jbiomech.2007.05.027.

[6] Boileau E, Nithiarasu P, Blanco PJ, Müller LO, Fossan FE, Hellevik LR, Donders WP, Huberts W, Willemet M, Alastruey J. A benchmark study of numerical schemes for one-dimensional arterial blood flow modelling. *International Journal for Numerical Methods in Biomedical Engineering* 2015; 31(10):e02732 (33 pages). doi:10.1002/cnm2732.